

# The density of mid-sized Kuiper belt object 2002 UX25 and the formation of the dwarf planets

M.E. Brown

*Division of Geological and Planetary Sciences, California Institute of Technology,  
Pasadena, CA 91125*

mbrown@caltech.edu

## ABSTRACT

The formation of the largest objects in the Kuiper belt, with measured densities of  $\sim 1.5 \text{ g cm}^{-3}$  and higher, from the coagulation of small bodies, with measured densities below  $1 \text{ g cm}^{-3}$  is difficult to explain without invoking significant porosity in the smallest objects. If such porosity does occur, measured densities should begin to increase at the size at which significant porosity is no longer supported. Among the asteroids, this transition occurs for diameters larger than  $\sim 350 \text{ km}$ . In the Kuiper belt, no density measurements have been made between  $\sim 350 \text{ km}$  and  $\sim 850 \text{ km}$ , the diameter range where porosities might first begin to drop. Objects in this range could provide key tests of the rock fraction of small Kuiper belt objects. Here we report the orbital characterization, mass, and density determination of the 2002 UX25 system in the Kuiper belt. For this object, with a diameter of  $\sim 650 \text{ km}$ , we find a density of  $0.82 \pm 0.11 \text{ g cm}^{-3}$ , making it the largest solid known object in the solar system with a measured density below that of pure water ice. We argue that the porosity of this object is unlikely to be above  $\sim 20\%$ , suggesting a low rock fraction. If the currently measured densities of Kuiper belt objects are a fair representation of the sample as a whole, creating  $\sim 1000 \text{ km}$  and larger Kuiper belt objects with rock mass fractions of 70% and higher from coagulation of small objects with rock fractions as low as those inferred from 2002 UX25 is difficult.

*Subject headings:* Kuiper belt: general — Kuiper belt objects: individual (2002 UX25) — planets and satellites: formation

## 1. Introduction

In standard accretionary scenarios for growth of objects in the Kuiper belt (i.e. Kenyon et al. 2008), the objects all form in regions of the nebula with similar physical characteristics and so should be composed of roughly similar amounts of rock and ice. It was surprising, therefore, to find that measured densities of Kuiper belt objects (KBOs) range from as low as  $0.5 \text{ g cm}^{-3}$  to at least  $2.6 \text{ g cm}^{-3}$  (Brown 2012).

A clear trend has emerged: the smaller objects have low densities, while larger objects have increasingly higher densities (Stansberry et al. 2006; Grundy et al. 2007; Vilenius et al. 2012; Fornasier et al. 2013). While larger objects often have higher densities due to pressure-induced phase changes, ice-rock bodies like these need to approach the size of Triton before this effect becomes significant (Lupo & Lewis 1979). A more likely culprit for the low densities of the small objects is porosity. Nothing is known about the porosity of KBOs, but in the asteroid belt the average porosity for objects as large as  $\sim 350 \text{ km}$  in diameter – the size of the small KBOs – has been calculated to be  $\sim 50\%$  (Baer et al. 2011), meaning that the compressed density of the object would be a factor of two higher than the measured density. Ice and rock compression experiments show that rock is capable of supporting much more porosity (Yasui & Arakawa 2009), so we regard asteroid porosities as a plausible upper limit to the porosities of icy KBOs. For this maximum porosity, the weighted average density for small KBOs of  $0.6 \text{ g cm}^{-3}$  corresponds to porosity-free density of  $\sim 1.2 \text{ g cm}^{-3}$ . Even for a high assumed porosity, these small KBOs have only about one third rock by mass. Simple coagulation of these rock-deficient objects will not lead to the much higher densities of the rock-rich dwarf planets.

With porosity the key unknown for small KBOs, an important clue to the formation of the dense dwarf planets would be the measurement of the densities of the smallest KBOs which are large enough to have had most of their porosity compressed out. Here we report the detection and orbital characterization of a satellite to the  $\sim 650 \text{ km}$  diameter hot classical KBO 2002 UX25. This object is an order of magnitude more massive than the next largest KBO with a measured density. We consider the effects of porosity on 2002 UX25, and we use the density we calculate for this system to attempt to understand the formation mechanism of the dwarf planets.

## 2. The orbit of the satellite of 2002 UX25

### 2.1. Hubble Space Telescope observations

A satellite of 2002 UX25 was discovered in observations from the High Resolution Camera (HRC) of the Advanced Camera for Surveys (ACS) of the Hubble Space Telescope (HST) on 26 August 2005. In order to determine the orbit of the satellite and the mass of the system, we obtained a series of 6 follow up observations a year later. For each observation we obtained 8 exposures of 275 second duration using the F606W filter.

The satellite is cleanly detected in 4 observations, undetected in 2 observations, and detected but blended with the primary in 2 observations (Figure 1). Astrometric positions of the satellite relative to 2002 UX25 were obtained following the method of (Brown et al. 2010), in which a five-times oversampled theoretical point spread function (PSF) is constructed for the pixel location of 2002 UX25 using TinyTim (Krist 1993), the HST PSF modeling software, and then the sub-pixel centers of 2002 UX25 and the satellite, the total flux of 2002 UX25 and the satellite, and the sky background are optimized using an iterative least-squares fit. We determine the uncertainties for each observation from the scatter of the positions measured in the 8 individual images acquired within a single HST orbit. We often detect motion consistent with the satellite orbital velocity within single sets of observations. To be conservative, however, we assume that all deviation within one orbit is due only to measurement error. Even in the most blended observation, we obtain consistent measurements in all 8 of the individual images during a single visit. The astrometric positions of the satellite are given in Table 1.

### 2.2. Keck laser guide star adaptive optics observations

The HST astrometric observations lead to a mirror ambiguity in the determination of the orbit pole (see below). For the 2002 UX25 system, breaking this ambiguity is particularly important; one orbital configuration would be undergoing current mutual events, while the other had its mutual event season before the satellite discovery. A single well placed astrometric point several years later could break this ambiguity. We obtained a single astrometric point using laser guide star adaptive optics (LGS AO) at the Keck Observatory (Wizinowich et al. 2006; van Dam et al. 2006) on 7 December 2012. Observations were scheduled for a night when 2002 UX25 passed within 35 arcseconds of an  $R \sim 13.7$  star that could be used for tip-tilt correction. We obtained a total of 73 individual 2 minute integrations of the system using the NIRC2 camera with a 0.02 arcsecond plate scale and the  $K_p$  filter. Image full-width-half-max (FWHM) measured on 2002 UX25 ranged from

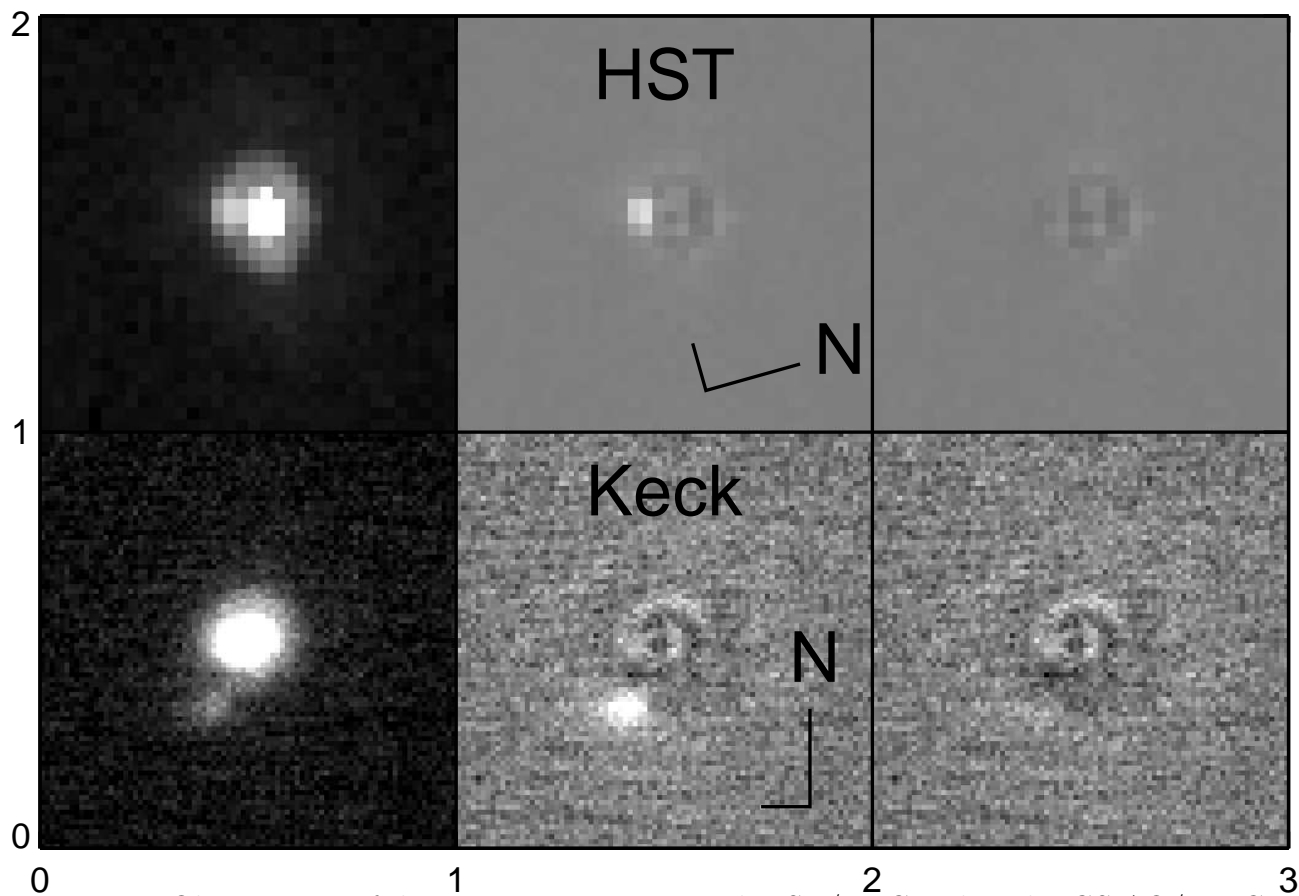


Fig. 1.— Observations of the 2002 UX25 system with HST/HRC and Keck LGS-AO/NIRC2. The northward orientation arrow is 0.25 arcseconds long, for scale. In the first column, we show the image of both 2002 UX25 and its satellite. From this image we simultaneously fit a PSF to both the primary and satellite. In the second column we show the image with the primary part of the fit subtracted. In the final column we show both components subtracted. The HST observation is from JD 2453939.98322 and is the most blended of the detections.

70 to 110 mas, worse than the 45 mas theoretical diffraction limit of a 10-meter telescope, but consistent with typical LGS AO performance with a moderate brightness off-axis tip-tilt star.

The satellite was visible in the best single 2 minute exposures and easily visible in all medianed stacks of five exposures (Figure 1). To accurately determine the astrometric position of the satellite we first selected the images with the best LGS AO correction. We determined the quality of the correction by fitting a single two-dimensional gaussian function at the position of the primary and calculating the average FWHM of the core. We then retained only the half of the data with a correction above the median value. These data were shifted to place the primary at a common position and then median-combined into 6 groups of 5.

While the satellite is outside of the core of the PSF, it is within the halo, which could affect measurements of its position. To accurately measure the position, we fit the primary and satellite with a PSF model that is the sum of two arbitrarily oriented two-dimensional Gaussian distributions. The residuals from these fits at the location of the satellite are nearly indistinguishable from background noise, thus the astrometric fits to the satellite position will no longer be affected by the halo of the primary PSF. As with the HST data, we determine the errors in the astrometric and photometric fits from the dispersion of the measures in the individual stacked frames (Table 1).

### 2.3. Orbit fits

It appears that the 2002 UX25 satellite is close to being in an edge-on orbit (Figure 2). Such an orbit is consistent with the 2 non-detections of the satellite in the HST data. We determine the best-fit orbit to the observations by using a Powell scheme to minimize the  $\chi^2$  value of the residuals and find the optimal orbital parameters. We ignore the non-detections, and note that all good fits naturally place the non-detections too close to the primary to have been observed. Our elliptical orbit has free parameters of semimajor axis, orbital period, inclination, longitude of the ascending node, mean anomaly, longitude of perihelion, and angle of nodes. The best fit has a  $\chi^2$  value of 2.97, or a reduced  $\chi^2$  for 5 degrees of freedom (6 sets of  $x, y$  coordinates minus 7 orbital parameters) of 0.6, suggesting that the uncertainties have indeed been overestimated. Forcing a fit to the mirror image orbit, we find a  $\chi^2$  value of 12.0, nearly four times higher than the best fit. As expected, the 2012 astrometry is the main discriminant between the two orbits. While the best fit orbit fits a position within 15 mas of the 2012 astrometric point, the mirror image orbit deviates by 92 mas, well outside of the uncertainty of the observation (Fig 2). We conclude that we

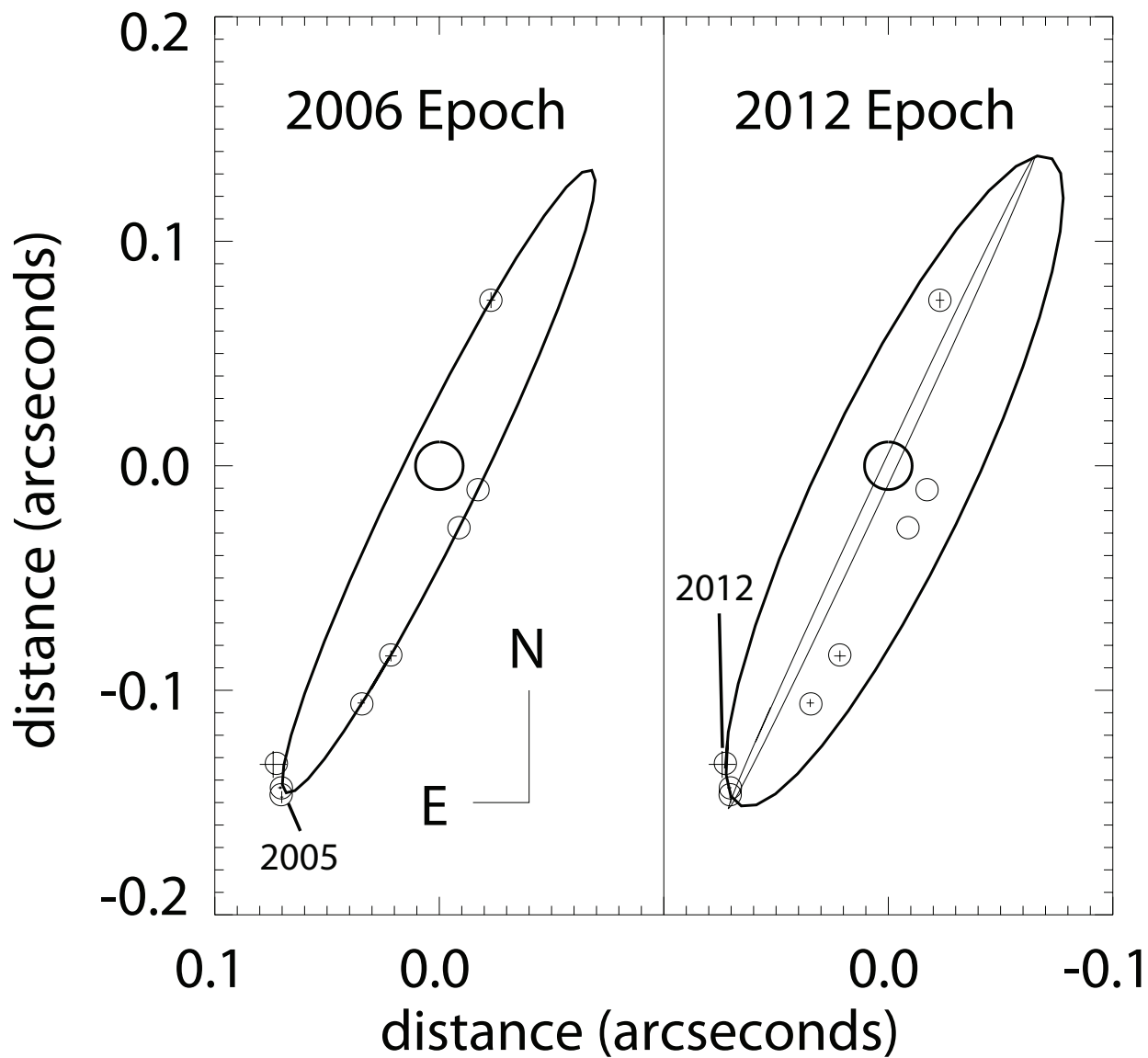


Fig. 2.— The orbit of the satellite of 2002 UX25 at the epoch of discovery and at the current epoch. The small circles show the predicted location of the satellite based on the best fit of all data from 2005-2012, while the crosses inside these circles show the observations and their uncertainties. For better visibility, the  $3\sigma$  uncertainties are shown. For the 2012 epoch, we show both the best fit orbit (thick line) and the mirror image orbit (thin line) which we exclude with high confidence. The large circle in the center shows the approximate size of 2002 UX25, while the small circles show the size of the satellite.

have resolved the mirror ambiguity and found the true orbital solution. The satellite plane crossed the line of sight to the earth and had mutual events in 2001. The next mutual event season does not occur until 2109.

The best-fit orbit has a moderate eccentricity of 0.17. Attempting a circular fit gives a best-fit  $\chi^2$  of 56.5, or a reduced  $\chi^2$  for 7 degrees of freedom of 8.1, significantly higher than for the elliptical fit. We conclude that the orbit is indeed elliptical.

We explore the uncertainties on the eccentricity and the other parameters by integrating through phase space using a Markov Chain Monte Carlo (MCMC) scheme. We use the Python package *emcee* (Foreman-Mackey et al. 2012) which implements the Goodman & Weare (2010) affine invariant ensemble sampler for MCMC. We assign uniform priors on all parameters (with two parameters being  $e \sin \omega$  and  $e \cos \omega$ , where  $e$  is the eccentricity and  $\omega$  is the argument of perihelion, rather than simply  $e$  and  $\omega$ ) and find good convergence with an ensemble of 100 chains running  $10^4$  steps with a initialization (“burn-in”) period, which is discarded, of 10% of the total length of each chain. The marginalized distribution of each of the parameters is nearly gaussian, we thus report the median and the middle 68.2% to represent the best fit plus  $1\sigma$  uncertainties (Table 2). We derive a marginalized system mass of  $1.25 \pm 0.03 \times 10^{20}$  kg, or about 0.7% the mass of Eris, the most massive known object in the Kuiper belt.

### 3. The size, density, and tidal evolution of 2002 UX25

Thermal radiometry of 2002 UX25 and its satellite has been obtained from both the Spitzer and Herschel Space Telescopes (Stansberry et al. 2008; Fornasier et al. 2013). A combined analysis using measurements at wavelengths from 24 to 500  $\mu\text{m}$  suggests an effective diameter of the system of  $692 \pm 23$  km with an albedo of  $10.7^{+0.5}_{-0.8}\%$ .

As the fractional brightness of the satellite measured with HST at visible wavelengths is comparable to that measured with Keck AO at infrared wavelengths (Table 2), with a mean value of 8% , it is plausible that 2002 UX25 and its satellite share the same surface characteristics and thus the same albedo. In this case we can estimate their separate diameters by assuming that the total thermal emission from each is proportional to their surface areas. Thus, the diameter of the primary would be  $\sim 664$  km while the satellite would be  $\sim 190$  km. Alternatively, if the satellite is assumed to have a  $\sim 5\%$  albedo typical of some smaller non-cold classical KBOs (Mommert et al. 2012; Vilenius et al. 2012; Santos-Sanz et al. 2012), the sizes would be  $\sim 640$  and  $\sim 260$  km, respectively. Assuming that the densities of the primary and satellite are identical, the densities for these two cases would be  $0.79 \pm 0.08$  and

$0.85 \pm 0.08 \text{ g cm}^{-3}$ , respectively. For simplicity, we will report the single average value with the full uncertainty range as  $0.82 \pm 0.11 \text{ g cm}^{-3}$ . 2002 UX25 is the largest object in the Kuiper belt with a measured density lower than  $1 \text{ g cm}^{-3}$ .

The eccentricity of  $0.17 \pm 0.03$  appears unusual for such a large object with a close satellite. For the size of 2002 UX25 and its satellite, we can estimate a time scale for damping of eccentricity by tides of the satellite of

$$\tau = -\frac{e}{\dot{e}} = \frac{4}{63} \frac{m_s}{m_p} \left(\frac{a}{r_s}\right)^5 \frac{\mu_s Q_s}{n},$$

where  $m_s$  and  $m_p$  are the satellite and primary masses,  $a$  is the semimajor axis,  $r_s$  is the radius of the satellite,  $Q$  is the tidal quality factor,  $n$  is the orbital angular frequency, and  $\mu_s$  is the effective rigidity of the satellite, defined as

$$\mu_s = \frac{19\mu}{2\rho g r_s},$$

where  $\mu$  is the material rigidity,  $\rho$  is the satellite density, and  $g$  is the satellite surface gravity (Murray & Dermott 2000). We find for 2002 UX25 an eccentricity damping time scale of  $\sim 4\left(\frac{\mu}{4 \times 10^9 \text{ N m}^{-2}}\right)\left(\frac{Q}{100}\right)$  Gyr, comparable to the age of the solar system for these reasonably assumed values of  $\mu$  and  $Q$  (Murray & Dermott 2000). The moderate eccentricity of the satellite of 2002 UX25, then, appears a reasonable outcome if the formation mechanism yielded an initially eccentric orbit or if eccentricity excitation ever occurred in the past.

#### 4. The densities of the Kuiper belt objects

We construct the size-density relationship for all objects with measured masses and sizes (Figure 3). We assume equal albedos and densities for all of the bodies in the system and derive the diameter and density of the primary object from the system mass and the measured effective diameter. System masses are taken from Rabinowitz et al. (2006), Buie et al. (2006), Brown & Schaller (2007), Grundy et al. (2007), Grundy et al. (2008), Benecchi et al. (2010), Brown et al. (2010), Grundy et al. (2011), Grundy et al. (2012), Stansberry et al. (2012) and Fraser et al. (2013), while effective diameters are from Stansberry et al. (2008), Vilenius et al. (2012), Mommert et al. (2012), Santos-Sanz et al. (2012), and Fornasier et al. (2013), with the combined Spitzer-Herschel results being used whenever available. For Orkus we derive densities for both the case where the albedos of the primary and satellite are assumed to be 23% (Fornasier et al. 2013) and for the case where the satellite has a more typical lower albedo of 5%, leading to a higher density for the system.

The low density of 2002 UX25 places strong constraints on any hypothesis proposed for the cause of the KBO size-density relationship. Objects of this size in the asteroid belt have

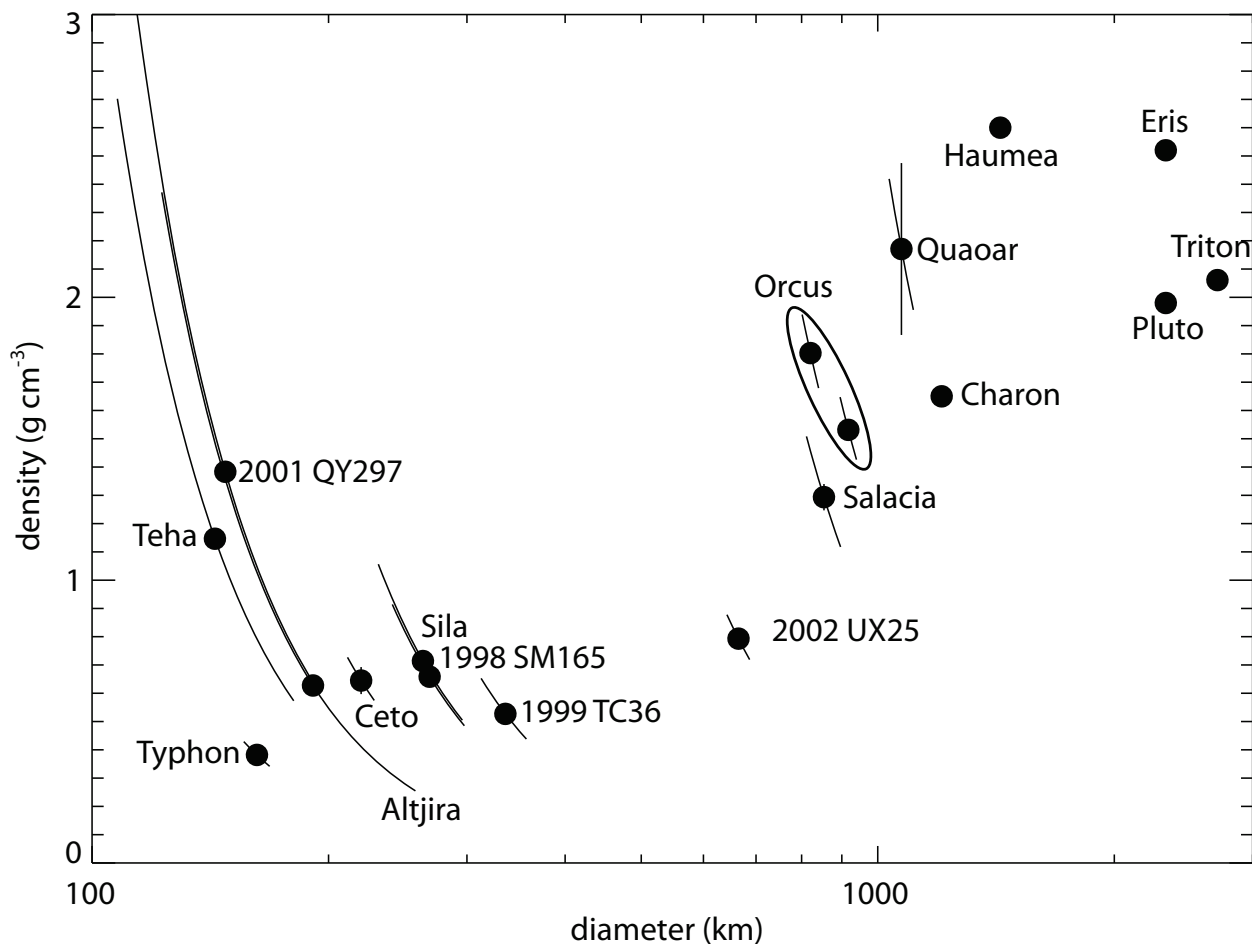


Fig. 3.— Densities of objects in and from the Kuiper belt. In most cases, the uncertainty in diameter is much larger than the uncertainty in mass, so the density-diameter uncertainty lies along a curved path. Quaoar has a larger mass uncertainty than most other objects, and that full uncertainty is shown as a vertical error bar at the position of Quaoar. Two possible density-radius solutions are shown for Orcus, one where Orcus and its satellite Vanth have equal albedos (the less dense solution) and one where Vanth has a lower albedo more typical of smaller KBOs (the more dense solution).

porosities of  $\sim 20\%$  and lower (Baer et al. 2011) In the Kuiper belt, porosities of objects this size should be lower; ice is more compressible at higher pressure (Yasui & Arakawa 2009), and *much* more compressible if the internal temperatures are elevated. Models of the internal structure of KBOs of this size range usually conclude that enough internal heating has occurred from radioactivity and accretional heating that liquid water is present at some point in the history of the object (see review by Prialnik et al. 2008). Bulk porosities, in that case, will be low.

While true porosities of cold icy large objects remain unmeasured, the analogies to stronger asteroids, the laboratory experiments, and the internal modeling all suggest that 2002 UX25 should not support significant bulk porosity. Assuming an upper limit of 20% for the porosity gives a compressed density of 2002 UX25 of close to  $1 \text{ g cm}^{-3}$ . Unless we have severely underestimated the porosity for this object, the rock fraction of 2002 UX25 is similar to the low rock fraction of the smaller KBOs.

## 5. Conclusions

The inferred low rock fraction of the 2002 UX25 system makes the formation of rock rich larger objects difficult to explain in any standard coagulation scenario. For example, to create an object with the volume of Eris would require assembling  $\sim 40$  objects of the size of 2002 UX25. Yet the assembled object, even with the additional compression, would still have a density close to  $1 \text{ g cm}^{-3}$  rather than the  $2.5 \text{ g cm}^{-3}$  density of Eris (Sicardy et al. 2011).

We offer a small number of possible ways in which the dwarf planets could still be created from the coagulation of smaller KBOs. First, it is possible that we have severely underestimated porosities. If 2002 UX25 could support a porosity of 50%, it would have a compressed density similar to that of Orcus or Charon. If the smaller objects have porosities of 60% or higher, they too would have a similar rock fraction to the smaller dwarf planets and coagulation would no longer present difficulties. The inferred change porosity from 2002 UX25 to Salacia to Orcus, over a relatively small range in diameter, would be unexpected. While such an extreme porosity for 2002 UX25 cannot be excluded, asteroid observations, internal modeling, and laboratory compression experiments all suggest that this possibility is unlikely.

The second manner in which dwarf planets could be built from small bodies is if the objects for which we have measured densities are not a fair sample of the Kuiper belt. Many – but not all – of the low density objects are part of the cold classical Kuiper belt, which is

known to have many distinct physical properties, including a larger fraction of satellites and thus a tendency to have a measured density (Noll et al. 2008). The objects Typhon and Ceto are both Centaurs, however, which are unlikely to be escapees from the stable cold classical region. The object 1998 SM165 is currently in a 2:1 resonance with Neptune, so its initial origin is more ambiguous. 2002 UX25, however, with an inclination of 19 degrees appears to be a clear member of the hot classical population. It is thus clear that low density small objects exist in the non-cold classical population of the Kuiper belt.

Another possibility is that there is a bias in our density measurements. If, for example, there were a significant population of higher density small objects with no density measurements, the large objects could easily be made. Density measurement requires the presence of a satellite. It is not impossible to imagine that perhaps less dense objects preferentially acquire satellites, but such a scenario seems contrived. Similarly, 2002 UX25 could be an outlier and not representative of the densities of the mid-sized KBOs. More density measurements in this size range are clearly warranted.

Finally, it is possible that objects of the dwarf planet size evolve to their high densities through the effects of giant impacts. Indeed, Haumea is thought to have lost much of its icy mantle, clearly leading to an increase in density (Brown et al. 2007), but giant impact modeling has not found a way to lose sufficient ice to affect the density enough to explain more than a small amount of the higher densities of the dwarf planets (Stewart & Leinhardt 2009; Leinhardt et al. 2010).

None of these alternatives appears likely. We are left in the uncomfortable state of having no satisfying mechanism to explain the formation of the icy dwarf planets. While objects up to the size of 2002 UX25 can easily be formed through standard coagulation scenarios, the rock rich larger bodies may require a formation mechanism separate from the rest of the Kuiper belt.

*Acknowledgments:* This research has been supported by grant NNX09AB49G from the NASA Planetary Astronomy program. Some of the data presented herein were obtained at the W.M. Keck Observatory, which is operated as a scientific partnership among the California Institute of Technology, the University of California and the NASA. The Observatory was made possible by the generous financial support of the W.M. Keck Foundation. Additional data were obtained from HST. Support for programs 10545 and 10860 were provided by NASA through a grant from the Space Telescope Science Institute, which is operated by the Association of the Universities for Research in Astronomy, Inc., under NASA contract NAS 5-26555. We thank the anonymous referee for thought provoking comments which substantially improved the presentation of this manuscript.

## REFERENCES

- Baer, J., Chesley, S. R., & Matson, R. D. 2011, *AJ*, 141, 143
- Benecchi, S. D., Noll, K. S., Grundy, W. M., & Levison, H. F. 2010, *Icarus*, 207, 978
- Brown, M. E. 2012, *Annual Review of Earth and Planetary Sciences*, 40, 467
- Brown, M. E., Barkume, K. M., Ragozzine, D., & Schaller, E. L. 2007, *Nature*, 446, 294
- Brown, M. E., Ragozzine, D., Stansberry, J., & Fraser, W. C. 2010, *AJ*, 139, 2700
- Brown, M. E. & Schaller, E. L. 2007, *Science*, 316, 1585
- Buie, M. W., Grundy, W. M., Young, E. F., Young, L. A., & Stern, S. A. 2006, *AJ*, 132, 290
- Foreman-Mackey, D., Hogg, D. W., Lang, D., & Goodman, J. 2012, *ArXiv e-prints*
- Fornasier, S., Lellouch, E., Müller, T., Santos-Sanz, P., Panuzzo, P., Kiss, C., Lim, T., Mommert, M., Bockelée-Morvan, D., Vilenius, E., Stansberry, J., Tozzi, G. P., Mottola, S., Delsanti, A., Crovisier, J., Duffard, R., Henry, F., Lacerda, P., Barucci, A., & Gicquel, A. 2013, *A&A*, 555, A15
- Fraser, W. C., Batygin, K., Brown, M. E., & Bouchez, A. 2013, *Icarus*, 222, 357
- Goodman, J. & Weare, J. 2010, *Communications in applied mathematics and computational science*, 5, 65
- Grundy, W. M., Benecchi, S. D., Rabinowitz, D. L., Porter, S. B., Wasserman, L. H., Skiff, B. A., Noll, K. S., Verbiscer, A. J., Buie, M. W., Tourtellotte, S. W., Stephens, D. C., & Levison, H. F. 2012, *Icarus*, 220, 74
- Grundy, W. M., Noll, K. S., Nimmo, F., Roe, H. G., Buie, M. W., Porter, S. B., Benecchi, S. D., Stephens, D. C., Levison, H. F., & Stansberry, J. A. 2011, *Icarus*, 213, 678
- Grundy, W. M., Noll, K. S., Virtanen, J., Muinonen, K., Kern, S. D., Stephens, D. C., Stansberry, J. A., Levison, H. F., & Spencer, J. R. 2008, *Icarus*, 197, 260
- Grundy, W. M., Stansberry, J. A., Noll, K. S., Stephens, D. C., Trilling, D. E., Kern, S. D., Spencer, J. R., Cruikshank, D. P., & Levison, H. F. 2007, *Icarus*, 191, 286
- Kenyon, S. J., Bromley, B. C., O’Brien, D. P., & Davis, D. R. *Formation and Collisional Evolution of Kuiper Belt Objects*, ed. M. A. Barucci, H. Boehnhardt, D. P. Cruikshank, A. Morbidelli, & R. Dotson, 293–313

- Krist, J. 1993, in *Astronomical Society of the Pacific Conference Series*, Vol. 52, *Astronomical Data Analysis Software and Systems II*, ed. R. J. Hanisch, R. J. V. Brissenden, & J. Barnes, 536–+
- Leinhardt, Z. M., Marcus, R. A., & Stewart, S. T. 2010, *ApJ*, 714, 1789
- Lupo, M. J. & Lewis, J. S. 1979, *Icarus*, 40, 157
- Mommert, M., Harris, A. W., Kiss, C., Pál, A., Santos-Sanz, P., Stansberry, J., Delsanti, A., Vilenius, E., Müller, T. G., Peixinho, N., Lellouch, E., Szalai, N., Henry, F., Duffard, R., Fornasier, S., Hartogh, P., Mueller, M., Ortiz, J. L., Protopapa, S., Rengel, M., & Thirouin, A. 2012, *A&A*, 541, A93
- Murray, C. D. & Dermott, S. F. 2000, *Solar System Dynamics*, ed. S. F. Murray, C. D. & Dermott
- Noll, K. S., Grundy, W. M., Stephens, D. C., Levison, H. F., & Kern, S. D. 2008, *Icarus*, 194, 758
- Prialnik, D., Sarid, G., Rosenberg, E. D., & Merk, R. 2008, *Space Sci. Rev.*, 138, 147
- Rabinowitz, D. L., Barkume, K., Brown, M. E., Roe, H., Schwartz, M., Tourtellotte, S., & Trujillo, C. 2006, *ApJ*, 639, 1238
- Santos-Sanz, P., Lellouch, E., Fornasier, S., Kiss, C., Pal, A., Müller, T. G., Vilenius, E., Stansberry, J., Mommert, M., Delsanti, A., Mueller, M., Peixinho, N., Henry, F., Ortiz, J. L., Thirouin, A., Protopapa, S., Duffard, R., Szalai, N., Lim, T., Ejeta, C., Hartogh, P., Harris, A. W., & Rengel, M. 2012, *A&A*, 541, A92
- Sicardy, B., Ortiz, J. L., Assafin, M., Jehin, E., Maury, A., Lellouch, E., Hutton, R. G., Braga-Ribas, F., Colas, F., Hestroffer, D., Lecacheux, J., Roques, F., Santos-Sanz, P., Widemann, T., Morales, N., Duffard, R., Thirouin, A., Castro-Tirado, A. J., Jelínek, M., Kubánek, P., Sota, A., Sánchez-Ramírez, R., Andrei, A. H., Camargo, J. I. B., da Silva Neto, D. N., Gomes, A. R., Martins, R. V., Gillon, M., Manfroid, J., Tozzi, G. P., Harlinton, C., Saravia, S., Behrend, R., Mottola, S., Melendo, E. G., Peris, V., Fabregat, J., Madiedo, J. M., Cuesta, L., Eibe, M. T., Ullán, A., Organero, F., Pastor, S., de Los Reyes, J. A., Pedraz, S., Castro, A., de La Cueva, I., Muler, G., Steele, I. A., Cebrián, M., Montañés-Rodríguez, P., Oscoz, A., Weaver, D., Jacques, C., Corradi, W. J. B., Santos, F. P., Reis, W., Milone, A., Emilio, M., Gutiérrez, L., Vázquez, R., & Hernández-Toledo, H. 2011, *Nature*, 478, 493

- Stansberry, J., Grundy, W., Brown, M., Cruikshank, D., Spencer, J., Trilling, D., & Margot, J.-L. 2008, in *The Solar System Beyond Neptune*, ed. M. A. Barucci, H. Boehnhardt, D. P. Cruikshank, & A. Morbidelli, 161–179
- Stansberry, J. A., Grundy, W. M., Margot, J. L., Cruikshank, D. P., Emery, J. P., Rieke, G. H., & Trilling, D. E. 2006, *ApJ*, 643, 556
- Stansberry, J. A., Grundy, W. M., Mueller, M., Benecchi, S. D., Rieke, G. H., Noll, K. S., Buie, M. W., Levison, H. F., Porter, S. B., & Roe, H. G. 2012, *Icarus*, 219, 676
- Stewart, S. T. & Leinhardt, Z. M. 2009, *ApJ*, 691, L133
- van Dam, M. A., Bouchez, A. H., Le Mignant, D., Johansson, E. M., Wizinowich, P. L., Campbell, R. D., Chin, J. C. Y., Hartman, S. K., Lafon, R. E., Stomski, Jr., P. J., & Summers, D. M. 2006, *PASP*, 118, 310
- Vilenius, E., Kiss, C., Mommert, M., Müller, T., Santos-Sanz, P., Pal, A., Stansberry, J., Mueller, M., Peixinho, N., Fornasier, S., Lellouch, E., Delsanti, A., Thirouin, A., Ortiz, J. L., Duffard, R., Perna, D., Szalai, N., Protopapa, S., Henry, F., Hestroffer, D., Rengel, M., Dotto, E., & Hartogh, P. 2012, *A&A*, 541, A94
- Wizinowich, P. L., Le Mignant, D., Bouchez, A. H., Campbell, R. D., Chin, J. C. Y., Contos, A. R., van Dam, M. A., Hartman, S. K., Johansson, E. M., Lafon, R. E., Lewis, H., Stomski, P. J., Summers, D. M., Brown, C. G., Danforth, P. M., Max, C. E., & Pennington, D. M. 2006, *PASP*, 118, 297
- Yasui, M. & Arakawa, M. 2009, *Journal of Geophysical Research (Planets)*, 114, 9004

Table 1: Separation of 2002 UX25 and its satellite

date (UT)	RA offset (mas)	dec offset (mas)	telescope/ instrument	relative brightness %
2453609.15758	70.2±0.3	-146±1	HST/HRC	8.9±0.5
2453939.30187	-	-	HST/HRC	-
2453939.98322	22±1	-85±1	HST/HRC	6.7 ± 0.2
2453944.04838	-23.0±0.9	74±2	HST/HRC	7.3±0.4
2453947.42261	-	-	HST/HRC	-
2453958.34814	70.8±0.5	-143.4±0.3	HST/HRC	8.8±0.2
2453965.20996	34.8±0.8	-105.7±0.9	HST/HRC	9.3±0.2
2456268.78992	74±3	-133±3	Keck/NIRC2	7.3±0.4

Table 2: Orbital parameters<sup>a</sup>

semimajor axis	4770±40 km
inclination	275.5±0.3 deg
period	8.3094±0.0002 days
eccentricity	0.17±0.03
argument of perihelion	254±1 deg
longitude of ascending node	23.3±0.3 deg
time of pericenter passage	JD 2453976.94±0.03
mass	1.25 ± 0.03 × 10 <sup>20</sup> kg
heliocentric orbit-satellite orbit angle	65 deg

<sup>a</sup>Relative to J2000 ecliptic